Electrical Power and Energy Systems 159 (2024) 110039

Contents lists available at ScienceDirect

International Journal of Electrical Power and Energy Systems

journal homepage: www.elsevier.com/locate/ijepes

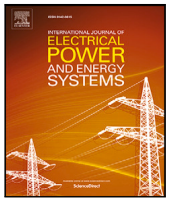

MPC-based control structure for high-power charging stations capable of providing ancillary services

Jonatan Ralf Axel Klemets *, Eirik Haugen, Bendik Nybakk Torsæter

SINTEF Energy Research, Trondheim, Norway

ARTICLE INFO

Keywords:
Model predictive control
Energy management system
High-power charging
Electrical vehicles
Ancillary services

ABSTRACT

The adoption of more electric vehicles (EVs) is going to pose some challenges for the grid due to the increase in demand for high-power charging. These issues will get further exacerbated with energy production moving from synchronous machines towards renewable energy sources (RES) with low inertia. High-power charging stations will thus, play a vital role since they can cause large power peaks but can also provide flexibility, especially if equipped with other resources, e.g., a battery energy storage system (BESS) and local energy production. These resources could be used for load shifting and to provide ancillary services for the grid if managed correctly.

This paper proposes a hierarchical control structure for operating a high-power charging station that can provide ancillary services. The control structure uses model predictive control (MPC) for economic management of the local resources while also controlling reactive and active power to improve the voltage quality. Additionally, a droop-based control is used to enable frequency support as an ancillary service. Finally, simulations show how the proposed control structure can improve the operation of the grid while simultaneously increasing the daily profits of the charging station by 20% compared to a rule-based control strategy and by over 35% when ancillary services also are provided.

1. Introduction

To effectively reduce carbon emissions, there is a need to increase the share of renewable energy sources (RES) and to further electrify the society [1,2]. However, the increased amount of RES and rapid development of the electrification of the transportation sector will create some challenges to the power system [3]. More energy generation from RES can result in reduced system stability and reliability due to the decline in system inertia caused by the smaller share of generation and load coming from synchronous (rotating) machines [4,5]. On the demand side, there is also expected to be an increase in higher power peaks at shorter time intervals from, e.g., fast charging of small- to medium-duty electric vehicles (EVs) [6] and high-power charging of heavy-duty EVs [7]. As a consequence, the reduced inertia combined with higher uncertainty and variations in load and production can lead to a faster rate of frequency deviations and varying voltage levels [8].

The transition from internal combustion engine vehicles to battery-electric vehicles will have an impact on the power system, as the energy now has to be served by the grid. Thus, EVs will require a network of high-power charging stations (HPCSs) to rapidly recharge their batteries when needed. This will impose significant demands on the distribution grid and can cause issues in power and voltage quality due to highly fluctuating loads, where voltage drops is one of the main issues caused by EV charging [9]. Also, the aggregated load from high-power charging often has a high peak-to-average power ratio, which implies a low utilization of the available grid capacity [6].

EVs can, however, be used to supply the grid with active power, a service which is commonly referred to as Vehicle-to-Grid (V2G). This allows EVs to provide ancillary services to the grid by temporarily discharging their batteries. Consequently, EV charging could potentially be used to improve the power quality in the grid, which was demonstrated in a recent Norwegian pilot study [10]. It has also been shown that providing ancillary services through V2G brings higher net present value (NPV) for the EV owners despite higher operational and capital costs [11]. However, when accounting for the battery energy storage system (BESS) degradation, the NPV will be lower due to the higher need for an initial investment [12]. Nevertheless, designing HPCSs such that they can provide ancillary services could benefit both the grid and the charging station operators, where a more extensive review of current V2G control methods can be seen in [13]. Unfortunately, EVs' departure time and charging demands at an HPCS are difficult to accurately predict, which makes it challenging for them to provide V2G service.

* Corresponding author.
E-mail address: jonatan.klemets@sintef.no (J.R.A. Klemets).

https://doi.org/10.1016/j.ijepes.2024.110039
Received 15 April 2022; Received in revised form 9 April 2023; Accepted 12 May 2024
Available online 20 May 2024

One solution is to combine the charging station with some additional energy storage system (ESS), which was proposed by [14] for charging EVs in parking lots and by [15] for fast charging stations. It was also concluded in [16] that a charging station without a BESS would have a negative grid impact regarding costs, emissions, and RES production. In addition to an ESS, a charging station can also be equipped with some local energy production. The optimal placement, design, and sizing for charging stations have been studied in, e.g., [17] using a graph-based approach and in [18], where the benefit of ridesharing was also considered. The authors of [19] investigated the optimal trade-off between the cost of electricity and the resulting pollution when designing a charging station. In [20], a method was proposed for the optimal design of a fast charging station when accounting for both the benefits for the charging station operators and the grid impacts. However, to manage HPCSs with multiple integrated energy sources that are capable of providing ancillary services, appropriate control systems must be used.

A prerequisite to optimally utilize HPCSs is that the chargers and the different resources are controllable and capable of providing stable and sufficiently fast responses to external signals. In [21], a control strategy of a bi-directional V2G charger was proposed, which was capable of providing the grid with active and reactive power. A sliding mode controller for bi-directional V2G chargers was designed in [22] to reduce the chattering effect caused by power converters. Local controllers for a BESS combined with fast charging were developed and tuned by [23] to improve the power quality. Similarly, a control algorithm was proposed in [24] for fast charging stations equipped with a flywheel energy storage system. A BESS controller was also developed in [25] for a photovoltaic power (PV) integrated charging station with the aim of smoothing the power output and avoiding overloading the transformer. These strategies focused on improving the power quality of the power converters and more stable internal voltage and current control of the charging stations. As a result, the chargers can more effectively respond to external control signals. However, little emphasis was put on how these external signals should be determined, which is typically the responsibility of an energy management system (EMS).

Microgrids usually use a hierarchical control structure, where the control system is split into different layers [26], with the EMS being a separate layer. In the context of EV charging, different hierarchical operation strategies of EV charging stations were reviewed in [27]. However, the focus was primarily on slow charging stations, such as parking lots, where EVs' arrival and departure times are known. In [28], a model predictive controller (MPC) was used to control the voltage by coordinating and using the reactive power for multiple charging stations in a distribution grid. An EMS to maximize the self-sufficiency of a residential charging station with a PV system was investigated in [29]. For individual HPCS, a rule-based EMS was proposed by [30], and a hierarchical controller for charging electric trucks was recently developed in [31]. An MPC was used by [31] to coordinate the EV charging with a BESS and a PV to reduce the charging costs without negatively impacting charging time.

1.1. Motivation of this research

The literature review shows an increasing interest in modeling, design, and placement of HPCSs, which can also be seen in a review on fast-charging stations [32]. The integration of RES and ESS with high-power charging is likely going to be necessary to meet the future load demand from EVs. Thus, it will be important to optimally design HPCSs such that both the charging demand and its grid impact are considered [20]. However, the optimal design of an HPCS and its resources is different from developing and implementing a suitable control system. Optimal design often assumes near-perfect knowledge of the load demands and the power generation potential, whereas a real-time control strategy must make decisions based on the limited information that is currently available.

Most of the EMSs or control strategies for HPCSs found in the literature do not consider both the charging operator's profitability and the grid impact. An exception is the coordination of multiple chargers in residential areas or parking lots that assume the arrival and departure times of the EVs are known [27–29]. However, EVs' exact arrival and departure times may not be known for an HPCS. Furthermore, coordination of charging stations requires the EMS for the individual HPCSs to adhere to some external control signal. Therefore, the EMS should, ideally, be designed to optimally control the power flows at the HPCS while simultaneously being adaptable to different and time-varying grid conditions.

A requirement for the EMS is that the chargers and the different resources can be controlled and are capable of providing sufficient fast and accurate responses. However, the design of low-level controllers for the power conversion within the HPCS and the evaluation of their accuracy and power losses are considered out of the scope for this work. Instead, the emphasis will be on developing an EMS for an individual HPCS and its associated energy resources that can benefit both the HPCS operator and the power system.

1.2. Novelty and contributions of this article

Rule-based control strategies [30] are unlikely going to archive optimal operation of an HPCS. Instead, optimization-based algorithms, such as an MPC used in [31], are better suited, especially when there is a need to coordinate multiple chargers with a BESS and a PV. However, the different objectives were weighted and solved in a single optimization problem, which makes tuning and providing ancillary services that require other time scales more challenging.

In [33], a single-layered MPC was used for charging unscheduled EVs while simultaneously providing voltage support by utilizing the available reactive power. As a result, more power could be made available to the EVs while keeping grid voltage within the allowed limits. However, similar to [31], other resources and the benefits of providing other ancillary services were not considered. Therefore, this article expands on the work in [33] by proposing a three-layered hierarchical control structure for an HPCS with both scheduled and unscheduled charging demands and different energy resources.

The control structure uses a two-layered MPC to predict and compute the economically optimal setpoints while ensuring that the voltage stays within specified limits by adjusting the active and reactive power flows. A droop controller is used to provide ancillary services that, when activated, will adapt the power demand at the charging station based on frequency deviations. As a result, the proposed controller for the HPCS will be able to contribute with both local voltage support for the distribution grid and frequency support for the transmission grid.

The controller was simulated on the grid model in [33], and the results showed how both the grid and the HPCS could benefit when using the proposed control strategy. The main contributions of this work are summarized in the following:

- A three-layered hierarchical control structure for controlling the chargers and associated resources at an HPCS that benefits both the HPCSs and the grid operators.
- A time-scale separation between the control layers for the HPCS, such that the controllers in each layer can be designed separately with their own objectives.
- An EMS framework for HPCSs to participate in the frequency regulation market by controlling it as a frequency-dependent load.
- A simulation study of the potential profitability from the proposed control structure compared with a simpler rule-based control strategy.

1.3. Paper organization

The structure of the paper is as follows: Section 2 provides some relevant background for this work. The proposed control structure is described in Section 3, where each individual control layer is explained separately, and a summary of the controller is provided at the end of the section. The resulting controller is simulated on a case study in Section 4, where its performance is compared with a rule-based controller. Finally, a discussion and a conclusion are provided in Section 5.

2. Background

When developing a control strategy, it is necessary to first know about the available and controllable assets at the charging station and how they influence the main grid. Additionally, the charging station's objectives, limitations, and requirements must be well defined and understood, especially if ancillary services are provided. Therefore, this section describes some background for the distribution system operator (DSO) interface, medium voltage (MV) grid, ancillary services, high-power charging stations, and model predictive control (MPC).

2.1. DSO interface and MV grid properties

For the DSOs, the main objective is to continuously supply the given load demand and at the same time keep the grid within defined limits on thermal capacity and voltage. As a result, the DSO must ensure that the power demand in the distribution grid is kept within an acceptable range to avoid that the grid voltage becomes too low or high. The relationship between the voltage (U_i) and the active (P_i) and reactive (Q_i) power in node i can be obtained using, e.g., the well-known power flow equations for a power network with n_{bus}-buses:

$$P_i = U_i \sum_{j=i}^{n_{bus}} Y_{ij} U_j \cos\theta_{ij} \tag{1}$$

$$Q_i = U_i \sum_{j=i}^{n_{bus}} Y_{ij} U_j \sin\theta_{ij}, \tag{2}$$

Here, Y_{ij} and θ_{ij} are the admittance and power angle between node i and j, respectively.

To avoid the voltage dropping too low, restrictions are usually placed on the HPCS of the amount of active power they can draw from the grid. However, HPCSs are, typically, connected to the MV grid that often has an R/X ratio close to one, which means both active and reactive power can significantly contribute to voltage control [34]. Therefore, having an HPCS inject reactive power while simultaneously consuming active power can improve the voltage quality of the grid without having to reduce its power demand [35,36].

In addition to voltage control, reactive power can also benefit the distribution grid in other ways, e.g., to minimize active power losses or to improve the power factor ($\cos\phi$) by reducing the reactive power exchange at the distribution and transmission connection [37]. However, this requires appropriate coordination and information sharing between the DSO and the flexible grid assets.

To utilize the flexibility potential in the distribution grid, appropriate markets or alternative systems for flexibility activation should be developed and implemented. E.g., local flexibility markets for congestion management could be used by consumers, producers, prosumers and aggregators.

Different market architecture and coordination schemes between the DSO and TSO have been suggested in [38], where a market model between EV aggregators and the grid operators was proposed in [39]. This could also potentially be extended to include HPCSs, but the development and comparisons of different market schemes are out of the scope of this paper. Nevertheless, it will be assumed that the future markets for ancillary services will operate with smaller time steps and shorter time periods between reserve allocation and activation.

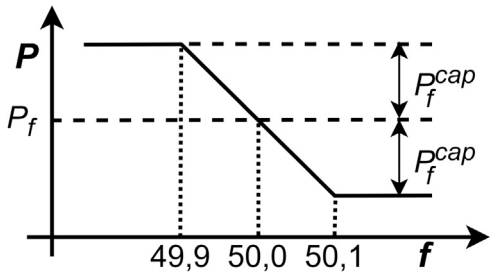

Fig. 1. Droop control characteristics for FCR-N provision. The power setpoint P_f for the generator changes linearly w.r.t. the deviation in frequency from its nominal value (50 Hz). The maximum change in P_f is set by the power capacity P_f^{cap}.

2.2. Ancillary services

Ancillary services, such as frequency control, are procured on the transmission grid level by the transmission system operator (TSO), where the frequency regulation usually consists of primary, secondary, and tertiary control. Here, the focus will be on the primary frequency control, denoted as frequency containment reserve (FCR), and more specifically, FCR-N, where "N" stands for normal.

In Norway, FCR-N is activated for normal deviations when the frequency varies between −0.1 and 0.1 Hz from its nominal value of 50 Hz. Thus, when providing frequency control, the power supplied or absorbed must react to the frequency deviations, which is done by droop controllers. Droop control only contains a proportional gain between frequency and the operational setpoint as seen in Fig. 1. When the frequency increases, the generation setpoint P_f is decreased such that the generator counteracts the increasing frequency. Similarly, if the frequency decreases, then P_f will increase.

Typically, FCR-N services are provided using synchronous machines at power plants. However, it is also possible to use a BESS or a flexible load. The use of BESS for providing ancillary services has been studied in [40,41]. The result from these studies shows great potential, as a BESS can give a very fast response and act similar to fast turbine governors, making them very efficient for providing primary frequency control services [40]. Therefore, there is a great potential of using EVs for frequency control which was shown in [42] to be economically beneficial for the EV owners. Similar economic benefits were also found by [43], where it was highlighted that the revenue could significantly be increased if bidirectional V2G chargers were used. Unfortunately, as of today, the power and energy requirements to participate in the Nordic balancing market exclude medium and small grid consumers and producers [44]. One possible solution is allowing multiple smaller actors to contribute to the frequency regulation by coordinating the load between the EVs using smarter local control strategies [45] or by having an aggregator that optimizes an aggregated EV fleet [46].

An HPCS could be used similarly, where the power requirement for the ancillary services is shared between multiple stations or other assets. However, this requires accurate information of available energy, and thus, uncertainties in the arrival and departure times of the EVs must be considered. Alternatively, if an HPCS is equipped with a BESS, it could guarantee a specific capacity that can be used for ancillary services whenever it is possible.

2.3. High-power charging station (HPCS)

Most of today's HPCSs can typically provide two types of charging services, which will be denoted as unscheduled charging (UC) and scheduled charging (SC). These consist of two different customer types, where UC is used by regular electric cars, whereas heavy EVs such as buses and trucks with more predictable schedules can use SC. As a result, their power requirements, charging time, and available flexibility

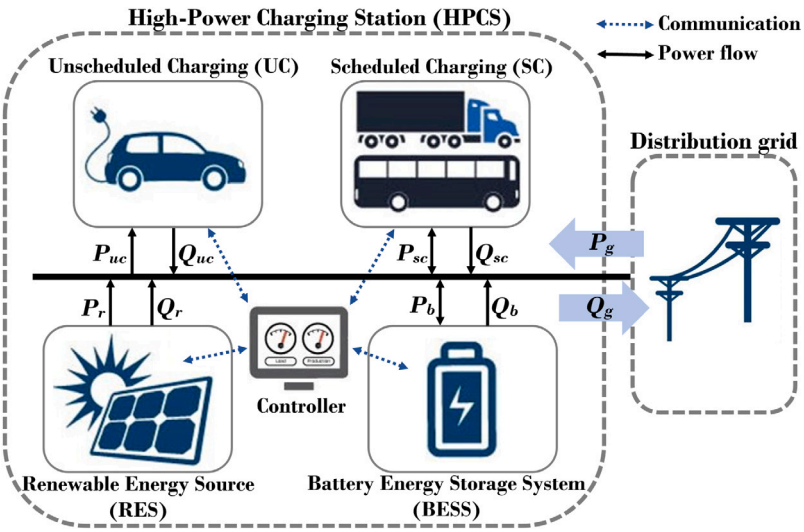

Fig. 2. Illustration of a high-power charging station with its different assets and power flows.

will differ. Therefore, there will be a difference in their objectives and how they should optimally be controlled.

As of today, the arrival and departure times, together with the charging demand for the individual EVs for UC, are unknown prior to their arrival. As a consequence, these loads will be very difficult to predict accurately, where typically, only an estimate based on, e.g., historical data will be available. Therefore, these loads have high uncertainty, which makes controlling and scheduling the HPCS more challenging. For SC, the arrival and departure times are assumed to be known together with their total energy demands and charging capabilities. As a result, they offer more flexibility and could potentially be used to provide V2G services.

In addition to the chargers, a charging station can also be equipped with some local energy production (e.g., a PV system) and a BESS, as depicted in Fig. 2. These provide additional flexibility, where in particular, the BESS is useful to deal with some of the uncertainty in the load demand. Furthermore, the BESS could also be used for arbitrage, voltage support, or other ancillary services, such as FCR-N, to increase the profitability of the charging station.

Modern chargers, BESS, and other distributed generation systems are often equipped with bi-directional converters that can operate in any of the four $P-Q$ quadrants. Therefore, both active and reactive power can contribute to the grid voltage, which increases the flexibility potential of an HPCS. This was utilized in [33], where an MPC algorithm was used to maximize the charging of EVs at an HPCS while using reactive power to keep the grid voltage within acceptable limits. In this paper, the MPC algorithm will be further developed to handle the different types of EV loads and to control a BESS and some local energy production.

2.4. Model predictive control

Model predictive control (MPC), sometimes also referred to as receding horizon control, is a popular control method that has received much attention in the control community [47,48]. An MPC can control multi-input and multi-output systems by repeatedly solving an optimization problem while simultaneously accounting for constraints. A generalized formulation of the MPC optimization problem for a prediction horizon of N samples can be given by

$$\underset{x,u}{\text{minimize}} \quad \sum_{k=1}^{N} J\Big(x(k), u(k), d(k)\Big) \tag{3a}$$

subject to

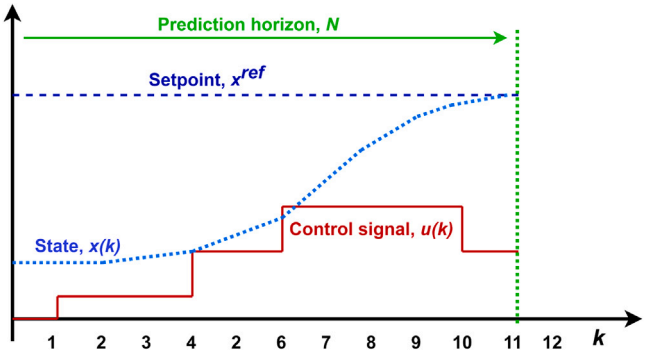

Fig. 3. Receding horizon operation of MPC. The optimal trajectories for the system states $x(k)$ and control signals $u(k)$ are computed at every time-step k for a given time horizon N and setpoint x^{ref}.

$$x(k+1) = \Phi\big(x(k), u(k), d(k)\big) \tag{3b}$$

$$\underline{x}(k) \le x(k) \le \overline{x}(k) \tag{3c}$$

$$\underline{u}(k) \le u(k) \le \overline{u}(k) \tag{3d}$$

Here, $J(\cdot)$ is the objective, and $\Phi(\cdot)$ is the dynamic model of the system, with x, u, and d being the states, control inputs, and disturbances, respectively. The upper and lower limits for the states and control inputs are given by $\{\underline{x}, \overline{x}\}$, and $\{\underline{u}, \overline{u}\}$.

A sequence of control actions is computed over the specified horizon window to give the optimal control trajectory, as illustrated in Fig. 3. However, from the computed control action sequence, only the first sample is implemented on the system. The model is then updated using the newly available information, and the control problem is solved again. This procedure is repeated continuously, and thus, it can update its control trajectory whenever new information becomes available. As a result, the MPC can adapt to prediction errors caused by, e.g., some model inaccuracies or unknown disturbances.

The MPC tries to steer the system towards some reference values x^{ref}, as seen in Fig. 3. However, this solution may not be optimal from an economic point of view since economics has often not been considered.

The concept of using an MPC with an economic objective is sometimes referred to as economic MPC (EMPC) [49]. Similar concepts as EMPC have been used [48] while still referring to it as MPC or receding horizon control. However, there are additional challenges when incorporating economics in the objective, e.g., closed-loop stability [49], and

thus, it is useful to separate the two. Even though closed-loop stability is not considered in this paper, MPC and EMPC will be distinguished to highlight their different objectives more clearly.

3. Proposed control structure

Designing a single controller capable of optimally controlling and scheduling a charging station and all its units is very difficult and would be extremely challenging to implement in practice. Therefore, a hierarchical control structure is proposed, inspired by the primary, secondary, and tertiary control that are commonly used by microgrids [26]. The control structure consists of three separate control layers that communicate with each other, but where each control layer has its own objectives and operates at different time scales. The different control layers and their objectives are:

1. **Economic model predictive control (EMPC) layer:** This layer focuses on the economics and optimal scheduling of the charging station. It uses energy prices and predictions of the future load demand and local power generation to determine the optimal state of charge (SoC) setpoints for the BESS and SC EVs. In addition, it continuously evaluates whether the charging station has the capacity to provide ancillary services and when it is economically beneficial.
2. **Model predictive control (MPC) layer:** The MPC layer controls and coordinates the BESS, the local energy production, and all the chargers at the charging station. Its main objective is to supply the charging EVs with the desired energy while also ensuring that the voltage stays within the allowable limits by controlling the active and reactive power flows. In addition, it tries to track the BESS setpoint provided by the EMPC layer. However, due to the stochastic nature of some of the EV load, it is allowed to deviate from the BESS setpoint when necessary.
3. **Droop control layer:** The final control layer consists of a droop controller that is used for FCR-N services. However, frequency support is only provided whenever the EMPC layer has determined it to be profitable and sufficient capacity is available at the charging station. Therefore, the droop controller requires an activation signal from the EMPC for it to become activated.

Fig. 4 gives an overview of the control structure, where each control layer operates at different time scales. Information and setpoints are shared between the layers and each controller receives relevant information and measurements of current states before making a new computation. Next, the individual control layers will be described in more detail.

3.1. EMPC layer

This layer consists of an EMPC, where the formulated optimization problem is based on the work in [12]. The economic objective with the horizon N_{empc} is defined as:

$$J_{EMPC} := \sum_{k=1}^{N_{empc}} \left[c_{spot}(k) P_g(k) \Delta t - c_{uc}(k) P_{uc}(k) \Delta t \right] - \sum_{k=1}^{N_{empc}} \left[b_f(k) c_f(k) \cdot P_f^{max} \Delta t \right]. \quad (4)$$

Here, c_{spot} is then energy cost (spot price), whereas c_{uc} is the compensation the HPCS receives for the power delivered to the UC EVs. P_g is the power from the grid, and P_{uc} is the power supplied to the UC EVs, with Δt being the sampling time. The terms b_f are binary decision variables that represent the times when the HPCS will provide FCR-N services with P_f^{max} being the maximum amount of power that the HPCS can allocate for FCR-N. The FCR-N price, c_f, determines the revenue received for providing the FCR-N services.

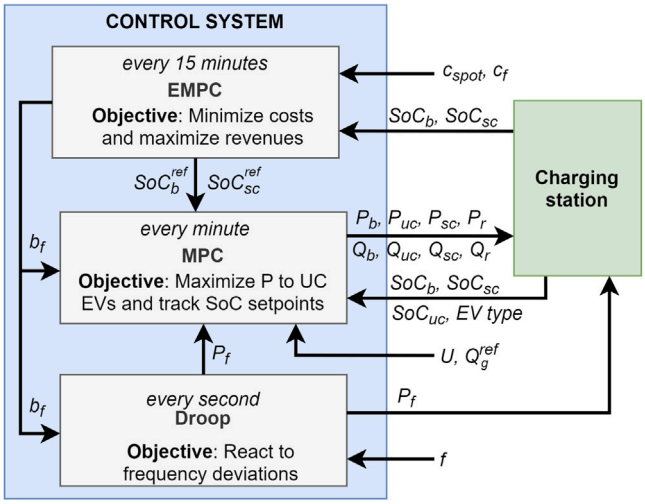

Fig. 4. Overview of the controller and the interaction between the layers.

The power balance at the charging station is ensured by

$$P_g(k) = P_{uc}(k) + \sum_{i=1}^{n_{sc}} P_{sc,i}(k) + P_b(k) - P_r(k), \quad (5)$$

where P_b, P_{sc}, and P_r are the powers absorbed or supplied by the BESS, the SC EVs, and the local energy generation, respectively. The subscript i in $P_{sc,i}$ represents the i:th charger.

The state of charge, SoC, in a battery is defined as its current energy level $E(k)$ divided by its full capacity (E_0):

$$SoC(k) = \frac{E(k)}{E_0} \quad (6)$$

Thus, the SoC dynamics for a battery can be modeled using the discrete-time state equation:

$$SoC(k+1) = SoC(k) + \frac{P(k)\Delta t}{E_0}, \quad (7)$$

where the charging and discharging efficiency will be assumed to be 100% for simplicity.

If a battery is going to provide ancillary services, it must ensure that at its current SoC, is capable of providing and absorbing sufficient power and energy for the worst-case situation. The SoC margin for frequency services, $0 \leq \varepsilon_f \leq 1$, ensures this by forcing the SoC to be at a level with sufficient range in both directions. The SoC margin is calculated from:

$$b_f(k) \cdot P_f^{max} \Delta t \leq \varepsilon_f(k) \cdot E_0. \quad (8)$$

To ensure that the SoC of the BESS is within the SoC margin for FCR-N services, ε_f will be included in the constraints that ensure that the SoC is kept within its minimum $\underline{SoC}$ and maximum $\overline{SoC}$ values:

$$\varepsilon_f(k) + \underline{SoC} \leq SoC(k) \leq \overline{SoC} - \varepsilon_f(k). \quad (9)$$

Additionally, when FCR-N services are provided, the grid power P_g should only vary according to the frequency deviations. Thus, when $b_f = 1$, the EMPC will assume the total load change ΔP_g is zero according to:

$$-\left(1 - b_f(k)\right)\overline{P}_g \leq \Delta P_g(k) \leq \left(1 - b_f(k)\right)\overline{P}_g \quad (10)$$

Using the objective function (4), the power balance expression (5), the SoC models, the constraints in (8)–(10) and the lower and upper limits, the EMPC will be formulated as:

$$\underset{P, SoC, b_f, \varepsilon_f}{\text{minimize}} \quad J_{EMPC} \quad (11a)$$

subject to

$$SoC_b(k+1) = SoC_b(k) + \frac{P_b(k)\Delta t}{E_{0,b}} \tag{11b}$$

$$SoC_{sc}(k+1) = SoC_{sc}(k) + SoC_0(k) + \frac{P_{sc}(k)\Delta t}{E_{0,sc}(k)} \tag{11c}$$

$$b_f(k) P_f^{max} \Delta t \leq \varepsilon_f(k) E_{0,b} \tag{11d}$$

$$\underline{SoC}_{sc}(k) \leq SoC_{sc}(k) \leq \overline{SoC}_{sc}(k) \tag{11e}$$

$$\varepsilon_f(k) + \underline{SoC}_b \leq SoC_b(k) \leq \overline{SoC}_b - \varepsilon_f(k) \tag{11f}$$

$$P_g(k) = P_{uc}(k) + \sum_{i=1}^{n_{sc}} P_{sc,i}(k) + P_b(k) - P_r(k) \tag{11g}$$

$$\big(1 - b_f(k)\big)\underline{P}_b \leq P_b(k) \leq \big(1 - b_f(k)\big)\overline{P}_b \tag{11h}$$

$$\underline{P}_{sc}(k) \leq P_{sc}(k) \leq \overline{P}_{sc}(k) \tag{11i}$$

$$0 \leq P_g(k) \leq \overline{P}_g \tag{11j}$$

$$-\big(1 - b_f(k)\big)\overline{P}_g \leq \Delta P_g(k) \leq \big(1 - b_f(k)\big)\overline{P}_g \tag{11k}$$

$$\Delta P_g(k+1) = P_g(k+1) - P_g(k) \tag{11l}$$

$$0 \leq P_r(k) \leq \hat{P}_r(k) \tag{11m}$$

$$0 \leq P_{uc}(k) \leq \hat{P}_{uc}(k) \tag{11n}$$

$$0 \leq \varepsilon_f(k) \leq 1 \tag{11o}$$

Here, SoC_b and SoC_{sc} is the SoC for the BESS and the SC EVs, respectively. The predicted load demand from the UC EVs are given by $\hat{P}_r$ and $\hat{P}_{uc}$ is the estimated power generation. $SoC_{sc}, SoC_0, E_{0,sc}, P_{sc} \in \mathbb{R}^{n_{uc}\times 1}$ are vectors, and thus, the division in (11c) should be considered as elemental-wise division, where SoC_0, and $E_{0,sc}$ are the SoC at arrival, and battery capacity of the SC EVs, respectively. These terms together with $\underline{SoC}_{sc}(k)$ and $\overline{SoC}_{sc}(k)$, are assumed to be known by the EMPC for the entire horizon, where $E_{0,sc}$ will always be set to a non-zero value to avoid zero division.

In (11h), the upper and lower charging rates for the BESS is multiplied with $(1 - b_f)$ to ensure the BESS is only planned to be use for FCR-N when b_f is active. Finally, an upper limit on the power exchange between the HPCS and the grid can be set by $\overline{P}_g$, which could also be a time-varying signal provided from an external source. Solving the optimization problem will give the lower layers with reference values for $SoC_b(1)$ and $SoC_{sc}(1)$, as well as a signal $b_f(1)$ if FCR-N services should be provided.

3.2. MPC layer

The role of the MPC layer is to try achieve the economic target computed by the EMPC by coordinating the chargers with the different assets at the HPCS. Thus, an objective function is formulated that minimizes the deviations from the setpoints given by the EMPC while simultaneously trying to provide the UC EVs with their desired charging power. The proposed objective function with the horizon N_{mpc} is given by

$$\begin{aligned} J_{MPC} := \sum_{k=1}^{N_{mpc}} \Bigg[& w_1 \Big(\overline{S}_{uc} - P_{uc}(k)\Big)^T \Big(\overline{S}_{uc} - P_{uc}(k)\Big) \\ & + w_2 \Big(SoC_{sc}^{ref}(k) - SoC_{sc}(k)\Big)^T \Big(SoC_{sc}^{ref}(k) - SoC_{sc}(k)\Big) \\ & + w_3 \Big(SoC_b^{ref}(k) - SoC_b(k)(k)\Big)^2 + w_4 \gamma_{sc}^T(k)\gamma_{sc}(k) \\ & - w_5 P_r^2(k) + w_6 \Big(Q_g^{ref}(k) - Q_g(k)\Big)^2 \Bigg], \end{aligned} \tag{12}$$

where $P_{uc} \in \mathbb{R}^{n_{uc}\times 1}$ is the active power delivered to the n_{uc} different UC EVs. The upper power limits of the chargers are denoted $\overline{S}_{uc} \in \mathbb{R}^{n_{uc}\times 1}$ and are included in the objective function to distribute power between the UC EVs equally. The SoC references that have been computed by the EMPC are given by SoC_b^{ref}, and SoC_{sc}^{ref} for the BESS, and SC EVs, respectively. The terms Q_g and Q_g^{ref} are the total amount of reactive power produced at the charging station, and its reference. The terms $\gamma_{sc} \in \mathbb{R}^{n_{sc}\times 1}$ are penalty variables that are used to discourage SoC_{sc} to go below their references.

The scalar weights w_1, w_2, w_3, w_4, w_5, and w_6 are used to assign different priorities to the different terms in the objective function. These weights will be set such that $w_4 > w_1 > w_3 > w_2 > w_5 > w_6$. Thus, the highest priority will be to ensure that the SoC of the SC EVs is charged above their references while trying to deliver as much power as possible to the UC EVs. The third priority is to keep the SoC for the BESS around its reference. However, this condition is less strict, and instead, the SoC_b is allowed to deviate from its reference to deal with the uncertainty in the load predictions by the EMPC. Both the terms P_r^2 and $(Q_g^{ref}(k) - Q_g(k))^2$, will have a relatively small weight compared to the other terms, since supplying reactive power has, as of today, no economic value for the charging station operator. Instead, Q_g will primarily be used to keep the voltage above a set threshold, thus, allowing more active power to be imported from the grid. The weight w_5 is of little importance, since increasing P_r will rarely conflict with the other objectives. Therefore, it will most of the time be at its maximum value, with potential exceptions when the voltage is too high or when FCR-N services are provided.

The active power balance, P_g, at the charging station used by the MPC is similar to the one for the in (5):

$$P_g(k) = \sum_{i=1}^{n_{uc}} P_{uc,i}(k) + \sum_{i=1}^{n_{sc}} P_{sc,i}(k) + P_b(k) - P_r(k) + P_f, \tag{13}$$

Here, the power delivered to each individual UC EV $P_{fc,i}$ has been included, instead of only having its aggregated value. The term P_f represents the power adjustments for the BESS when the charging station provides FCR-N services. In addition to the active power balance, the MPC layer will also include the reactive power balance Q_g:

$$Q_g(k) = \sum_{i=1}^{n_{uc}} Q_{uc,i}(k) + \sum_{i=1}^{n_{sc}} Q_{sc,i}(k) + Q_b(k) + Q_r(k), \tag{14}$$

The SoC dynamics for the BESS and EVs are the same as in (7) for the MPC but with a faster sampling time, Δt. The slack variable, γ_{sc}, from the objective function (12) will be included in the constraint,

$$SoC_{sc}(k) \geq SoC_{sc}^{ref} - \gamma_{sc}, \tag{15}$$

to penalize deviations from the reference. Thus, $\gamma_{sc} \geq 0$ whenever the SC EVs are not charged to or above SoC_{sc}^{ref}, which will increase the cost in (12).

To maximize the profitability, the UC EVs should be charged with as much power as possible for the time they are occupying a charger. Hence, the first term in (12). However, the EVs will rarely be able to charge at the maximum power capability, since the allowed charging rate for an EV depends on the EV model and its battery. Instead, the allowed power input to the EV battery is determined by the battery management system and depends on different factors such as SoC and temperature. As in [33], the allowed charging rate will be constrained by the power curves in Fig. 5. Based on these power curves, the maximum power constraint will be simplified to piecewise linear functions

$$\overline{P}_{uc}(k) := \alpha \odot SoC_{uc}(k) + \beta, \tag{16}$$

where $\odot$ is the element-wise product and $\alpha, \beta \in \mathbb{R}^{n_{uc}\times 1}$ are constants, depending on the EV models and their current SoC.

A voltage model can obtained using the power flow equations in (2). However, these equations are nonlinear and can be challenging to solve. Thus, to reduce the computational complexity, the power flow equations in (2) are linearized around the nominal operating point (e.g., at the base load demand of the network):

$$\begin{bmatrix} \Delta P \\ \Delta Q \end{bmatrix} = \mathcal{J} \begin{bmatrix} \Delta U \\ \Delta \theta \end{bmatrix}, \text{ where } \mathcal{J} := \begin{bmatrix} \frac{\partial P}{\partial U} & \frac{\partial P}{\partial \theta} \\ \frac{\partial Q}{\partial U} & \frac{\partial Q}{\partial \theta} \end{bmatrix}. \tag{17}$$

The resulting Jacobian matrix $\mathcal{J}$ can be inverted to describe the influence ΔP and ΔQ have on ΔU and $\Delta\theta$:

$$\begin{bmatrix}\Delta U\\ \Delta\theta\end{bmatrix} = \mathcal{J}^{-1}\begin{bmatrix}\Delta P\\ \Delta Q\end{bmatrix}, \text{ where } \mathcal{J}^{-1} := \begin{bmatrix}\frac{\partial U}{\partial P} & \frac{\partial U}{\partial Q}\\ \frac{\partial\theta}{\partial P} & \frac{\partial\theta}{\partial Q}\end{bmatrix}. \tag{18}$$

By ignoring the power angles, θ, and only considering the elements in ΔU and $\mathcal{J}^{-1}$ that correspond to the node of the charging station, a model for the voltage U can be given by

$$U(k+1) = U(k) + \frac{\partial U}{\partial P}\Delta P(k) + \frac{\partial U}{\partial Q}\Delta Q(k). \tag{19}$$

Using the objective function in (12), the SoC models, the voltage model, the upper power curve for UC EVs in (16) and some additional upper and lower constraints, the MPC formulation can be given by:

$$\underset{P,Q,SoC,U}{\text{minimize}} \quad J_{MPC} \tag{20a}$$

subject to

$$SoC_b(k+1) = SoC_b(k) + \frac{P_b(k)\Delta t}{E_{0,b}} \tag{20b}$$

$$SoC_{sc}(k+1) = SoC_{sc}(k) + \frac{P_{sc}(k)\Delta t}{E_{0,sc}(k)} \tag{20c}$$

$$SoC_{uc}(k+1) = SoC_{uc}(k) + \frac{P_{uc}(k)\Delta t}{E_{0,uc}(k)} \tag{20d}$$

$$P_g(k) = \sum_{i=1}^{n_{uc}} P_{uc,i}(k) + \sum_{i=1}^{n_{sc}} P_{sc,i}(k) + P_b(k) - P_r(k) + P_f \tag{20e}$$

$$Q_g(k) = \sum_{i=1}^{n_{uc}} Q_{uc,i}(k) + \sum_{i=1}^{n_{sc}} Q_{sc,i}(k) + Q_b(k) + Q_r(k) \tag{20f}$$

$$U(k+1) = U(k) - \frac{\partial P}{\partial U}\Delta P_g(k) - \frac{\partial P}{\partial U}\Delta Q_g(k) \tag{20g}$$

$$-\big(1-b_f(k)\big)\overline{P}_g \le \Delta P_g(k) \le \big(1-b_f(k)\big)\overline{P}_g \tag{20h}$$

$$\Delta P_g(k+1) = P_g(k+1) - P_g(k) \tag{20i}$$

$$\Delta Q_g(k+1) = Q_g(k+1) - Q_g(k) \tag{20j}$$

$$\underline{SoC}_b(k) \le SoC_b(k) \le \overline{SoC}_b(k) \tag{20k}$$

$$\underline{SoC}_{sc}(k) \le SoC_{sc}(k) \le \overline{SoC}_{sc}(k) \tag{20l}$$

$$SoC_{sc}(k) \ge SoC_{sc}^{ref} - \gamma_{sc} \tag{20m}$$

$$\underline{P}_b \le P_b(k) + P_f \le \overline{P}_b \tag{20n}$$

$$\underline{P}_{sc}(k) \le P_{sc}(k) \le \overline{P}_{sc}(k) \tag{20o}$$

$$0 \le P_{uc}(k) \le \alpha \odot SoC_{uc}(k) + \beta \tag{20p}$$

$$0 \le P_r(k) \le \overline{P}_r \tag{20q}$$

$$P_g(k) \le \overline{P}_g \tag{20r}$$

$$P_b^2 + Q_b^2 \le \overline{S}_b^2 \tag{20s}$$

$$P_{sc}^2 + Q_{sc}^2 \le \overline{S}_{sc}^2 \tag{20t}$$

$$P_{uc}^2 + Q_{uc}^2 \le \overline{S}_{uc}^2 \tag{20u}$$

$$P_r^2 + Q_r^2 \le \overline{S}_r^2 \tag{20v}$$

$$\underline{U} \le U(k) \le \overline{U} \tag{20w}$$

Most of the constraints in (20b)–(20w) are either identical or very similar to (11b)–(11o) but with faster sampling time. However, the MPC also considers the physical effects and restriction of the distribution grid by inclusion of a voltage model (20g) and voltage constraints (20w), as well as reactive power (20f) and the power rating for the inverters (20s)–(20w).

Solving (20b)–(20w), provides the active power and reactive power setpoints for all the scheduled and unscheduled charging EVs, as well as for the BESS and the RES.

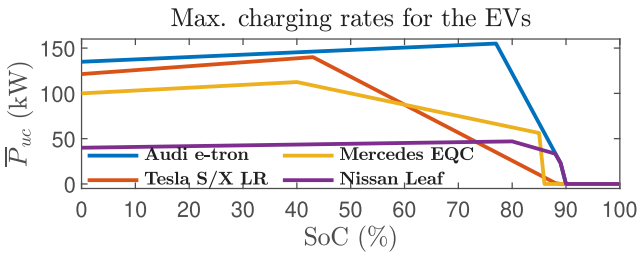

Fig. 5. Maximum charging rate curves for the EV batteries [50].

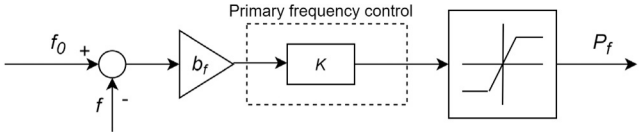

Fig. 6. Droop control implementation for FCR-N.

3.3. Droop control layer

The droop control is based on the regulation strategy in Section 2.2 and the primary frequency control in [40], as illustrated in Fig. 6. The power output P_f from the droop controller can thus be computed using:

$$P_f = K \cdot b_f \cdot (f_0 - f) \tag{21}$$

where f_0 and f are the nominal and measured frequency, respectively. The difference in frequency gets multiplied with the regulation gain K and the binary activation variable b_f, where b_f will be received from the EMPC layer. Thus, P_f will be zero unless the EMPC layer has determined that FCR-N services should be provided. The saturation block in Fig. 6 ensures that the frequency provision is within the allowable range P_f^{max}, as defined by the max capabilities of the charging station. Therefore, the gain K should also be set such that P_f equals P_f^{max} for max allowed frequency deviation.

The droop output P_f is used to adjust the setpoint for the BESS according to the frequency deviations such that the actual setpoint becomes $P_f + P_b$, where P_b is computed by the MPC. Thus, P_f will also be sent to the MPC layer and included in (20e) and (20n).

3.4. Controller summary

One of the main advantages of the proposed three-layer control structure is the time-scale separation between the layers. Thus, the EMPC layer can focus on the economically optimal control and scheduling for a longer prediction horizon, whereas the MPC layer can adapt to faster changes such as voltage fluctuations and changes in load demand. Consequently, they solve different optimization problems. The EMPC solves a mixed-integer linear program (MILP), while the MPC solves a quadratically constrained quadratic program (QCQP) problem due to the constraints in (20s)–(20w).

When ancillary services are to be provided, both the MPC and the droop layer receive a signal b_f from the EMPC layer. During this time, the MPC tries to keep the power exchange with the grid, P_g, at a constant value, while the droop controller adjusts P_g by manipulating P_f based on the frequency deviations. This will later be illustrated in Section 4.2 and Fig. 9. The droop control signal P_f will adjust the setpoint to the BESS on a significantly faster time-scale than the MPC layer. However, the MPC may later shift these loads by, e.g., manipulating P_b as long as P_g in (20e) remains unchanged.

4. Case study

The proposed control structure was simulated in Matlab and Simulink using YALMIP [51], where the EMPC problem in (11a)–(11o)

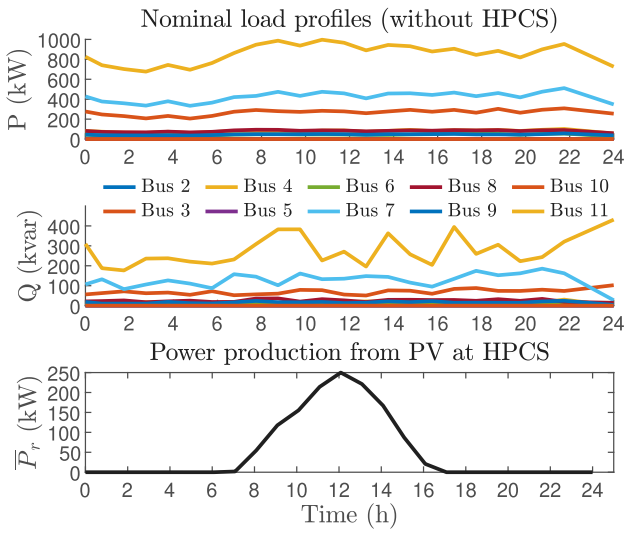

Fig. 7. Load profiles for the distribution grid and the maximum power production from the PV system.

and the MPC problem in (20a)–(20w) are solved using the open-source solvers SDPT3 [52] and lpSolve [53], respectively. The time horizon for the EMPC was set to 24 h with a sampling time of 15 min, whereas the MPC uses a 1 min sampling time and a 15 min time horizon.

Simulations are made on the same grid model that was used in [33]. The model is based on a real 22 kV radial distribution grid that consists of 11 different buses, where seven of them are connected to some time-varying load shown in Fig. 7. As in [33], the charging station will be placed at bus 10, but for more information about the grid topology, the cross-section of the lines, and admittances, the reader is referred to [6,33].

The charging costs for the UC EVs will be set to a constant value of 0.1 €/kWh, whereas the energy (spot) and FCR-N prices used in the simulations can be seen in Fig. 8 [54], where it will be assumed that all bids for FCR-N services will be accepted at the given price. The required power capacity P_f^{max} to participate in the FCR-N market has been set to 250 kW, and it is assumed that the HPCS can cancel or make a bid up to 1 h before the time of activation.

4.1. HPCS and EV queuing model

The HPCS consists of ten 150 kVA chargers for UC EVs and two 300 kVA chargers for SC EVs. The same EV fleet and queuing model as in [33] will be used for the UC EVs, where their arrival rate to the charging station varies during the day. When an UC EV arrives, it will occupy the first available charger to start charging until it reaches an SoC of 90 %, or until the duration it has been occupying the charger exceeds 1 h. If multiple EVs want to charge simultaneously, a queue will start to form and EVs will be forced to wait until a charging spot becomes available. For these simulations, the maximum waiting time for the EVs has been set to 15 min, i.e., an EV will leave the queue after 15 min, and the charging station will lose a customer. For more information about the queuing model, and the number of EVs that will be visiting the charging station, the reader is referred to [33].

For the UC EVs, information about the individual EV model, arrival/departure time, and charging demand is unknown to HPCS, but an estimate of their total load demand is available. However, for the SC EVs, information about their battery size, arrival/departure time, SoC at arrival, and desired SoC at departure is assumed to be known. For the simulated day, a total of five SC EVs will be charging. They all have the same size battery (500 kWh), initial SoC (25%), and target SoC (80%), but their arrival and departure times vary.

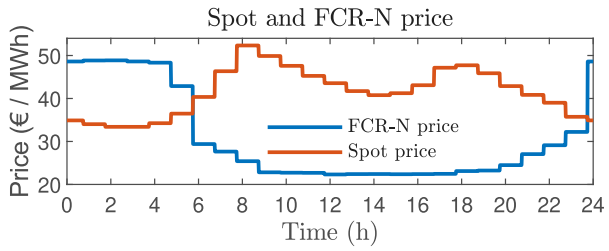

Fig. 8. Spot prices and FCR-N prices used for the case study [54].

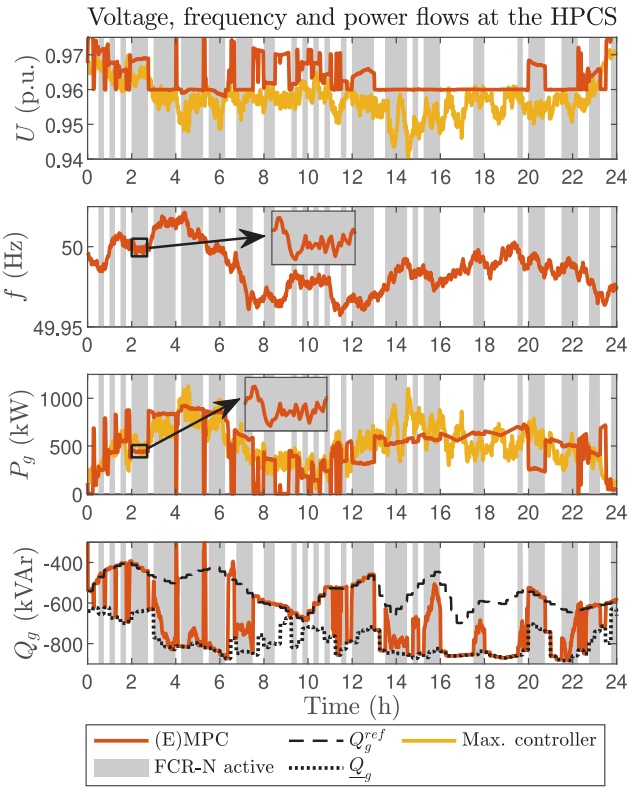

Fig. 9. Total power flows (P_g and Q_g), voltage (U) and frequency (f) at the HPCS when using the max controller and the proposed (E)MPC.

The HPCS model is also equipped with 1.5 MWh BESS and a PV-system, where the maximum possible power generation for the simulated day is shown in Fig. 7.

4.2. Simulation and results

The HPCS is simulated for 24 h, where the proposed hierarchical (E)MPC controller is compared to two simpler control strategies to demonstrate its benefits. The two alternative control strategies and their algorithms can be described by

1. Maximum capacity control strategy (Max. controller):
   - Charges SC EVs with a constant rate.
   - Supplies UC EVs with max. charging rates $\overline{P}_{uc}$
   - Does not use BESS
   - Does not consider any voltage restrictions
2. Rule-based control strategy (RBC):
   - Charges SC EVs with a constant rate.
   - Charges UC EVs with max $\overline{P}_{uc}$, when possible

Table 1
Total energy from the grid and energy provided to the UC EVs with the daily profits for the simulated controllers, together with the average value of $\cos\phi$ with ± 2 standard deviations.

Control method	Energy from grid	Energy to UC	Energy cost	UC revenue	FCR-N revenue	Profit	$\cos\Phi$
Max. controller	12.27 MWh	12.18 MWh	504 €	1218 €	0	714 €	0.971 ± 0.017
Rule-based control	9.54 MWh	9.69 MWh	382 €	969 €	0	587 €	0.969 ± 0.014
(E)MPC w/o FCR-N	11.73 MWh	11.87 MWh	475 €	1187 €	0	711 €	0.997 ± 0.006
(E)MPC	11.98 MWh	11.87 MWh	487 €	1187 €	102 €	802 €	0.998 ± 0.006
(E)MPC with error	12.00 MWh	11.87 MWh	486 €	1187 €	93 €	793 €	0.998 ± 0.006

- Charges BESS if $SoC \leq 80\%$ and $U \geq \underline{U}$
- Discharges BESS if $SoC \geq 20\%$ and $U \leq \underline{U}$
- Reduces P_{uc} if $SoC \leq 20\%$ and $U \leq \underline{U}$

Neither of these two control strategies utilizes reactive power, but both will control the PV system at its maximum $\overline{P}_r$.

Fig. 9 shows the active power drawn from the grid P_g and the voltage U at the HPCS when using the max controller and the proposed E(MPC) control structure. The lower threshold for the voltage $\underline{U}$ has been set to 0.96 p.u. as this ensures the voltages are kept within acceptable limits for the downstream buses. As seen in Fig. 9, when simply running the HPCS at max capacity, the voltage will significantly drop below the allowed limit. However, the proposed E(MPC) controller can keep the voltage above the set threshold by shifting the active power loads and utilizing the available reactive power Q_g.

The reference Q_g^{ref} together with the maximum $\overline{Q}_g$ and minimum $\underline{Q}_g$ can be decided externally by, e.g., the DSO, to improve the grid performance. Here, these values have been computed to minimize the reactive power exchange between the distribution and transmission system, i.e., to improve the power factor $\cos\phi$ at the distribution and transmission grid connection. Thus, the aim of Q_g^{ref} is to get $\cos\phi = 1$, whereas $\underline{Q}_g$ is set to ensure $\cos\phi \geq 0.95$. As a result, the reactive power Q_g from the E(MPC) in Fig. 9, is kept above $\underline{Q}_g$ while also trying to follow Q_g^{ref} whenever it does not negatively impact the voltage nor the profits of the HPCS.

The grayed areas in Fig. 9 show the times when the (E)MPC provides FCR-N services, for economic reasons. During this time, the HPCS will act as a constant load that only varies based on the frequency deviations. This is illustrated in the highlighted areas after 2 h mark for the frequency and P_g, where it can be seen how P_g follows the frequency deviations.

Fig. 10 shows the total power supplied to the UC EVs together with the SoC for the BESS, and the SC EVs, respectively. Here, the performance of two different (E)MPCs has also been compared; one that provides FCR-N and one that does not. All the compared controllers are able to supply the UC EVs with almost identical P_{uc} until around the 11th hour. At which the RBC must reduce P_{uc} to avoid the voltage dropping below 0.96 p.u. since the SoC of the BESS is at 20%. However, both (E)MPC controllers are able to charge the UC EVs at near maximum capacity by using reactive power and by temporarily shifting active power from the SC EVs, while the two simpler controllers charge them at a constant rate.

The E(MPC) used for the results in Fig. 10 assumes perfect prediction of the load demand from the UC EVs. However, perfect estimates of load demand for a given day are likely not going to be available. Consequently, there will be prediction errors, which will impact the performance of the (E)MPC. Thus, a simulation was made using an imperfect load estimate for the UC EVs. The results can be seen in Fig. 11 and shows that the (E)MPC is still able to charge the UC EVs at near their maximum capacity despite the prediction errors. However, there will be a decrease in revenue from FCR-N services, since the SoC of the BESS will have to deviate more from its setpoint to compensate for the prediction errors. As a result, there will be less capacity available for FCR services.

Table 1 shows the total energy imported from the grid and supplied to the UC EVs together with their total cost and revenues for the different controllers. The revenue from the FCR-N services has also been included, as well the power factor $\cos\phi$ at the connection point of the distribution and transmission grid. The max controller generates the most revenue from the UC EVs, but the resulting voltage drop would not be allowed by the DSOs. Using a BESS with the RBC keeps the voltage within the allowable range but fails to maximize the profitability of the HPCS. The proposed (E)MPC keeps voltage above the threshold and improves the grid performance $\cos\phi$ while achieving similar profits as the max controller. The profits are further increased if the (E)MPC is allowed to provide ancillary services. Prediction errors of the load will reduce the (E)MPC profits, but they were still higher compared to the other strategies.

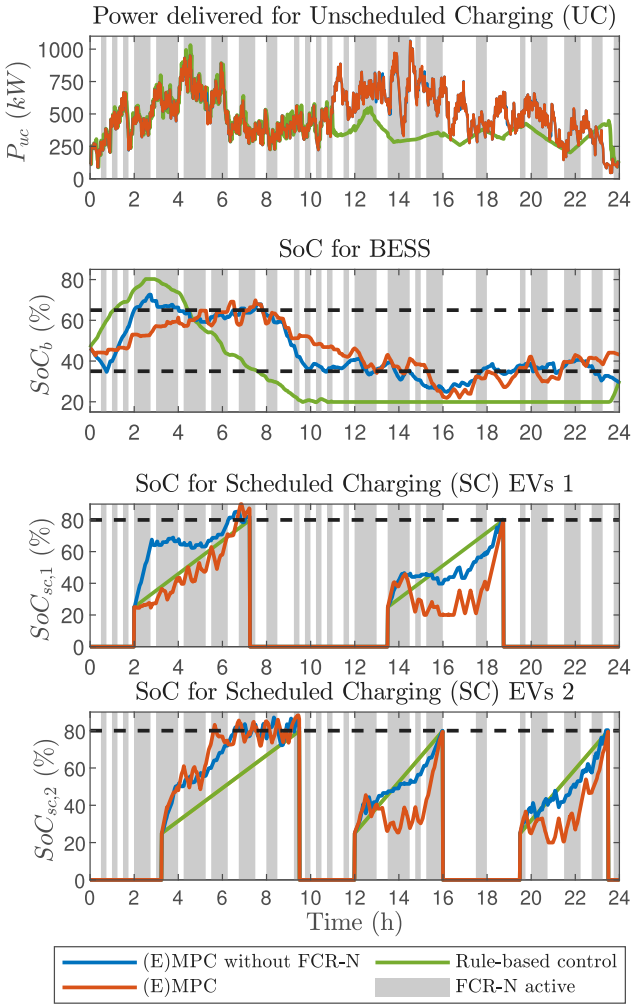

Fig. 10. Power supplied to the UC EVs and the SoC for the BESS and SC EVs. P_{uc} is almost identical for the controllers except for RBC, and thus, they overlap. The dashed line for the BESS is the SoC capacity required for FCR-N and the dashed lines for the SC EVs are their targeted setpoints.

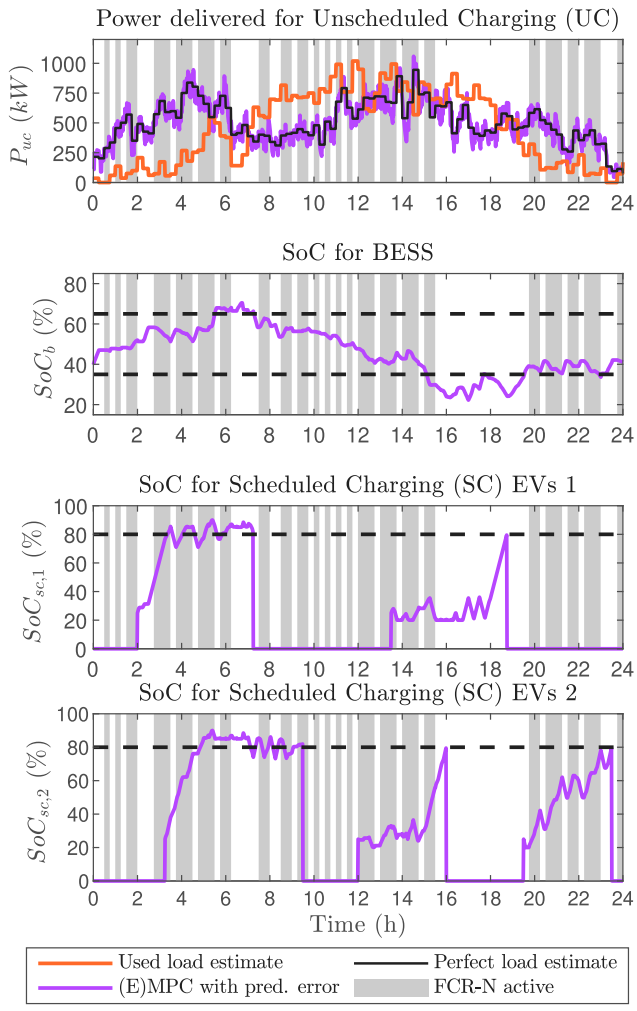

Fig. 11. Power supplied to the UC EVs and the SoC for the BESS and SC EVs when using the (E)MPC with incorrect load predictions.

5. Discussion and conclusion

HPCSs are often seen as a big challenge to the power grid due to their large and intermittent power demand. However, a charging station can also be seen as a flexible resource that provides ancillary services, such as FCR, or helps stabilize the voltage, using a combination of active and reactive power. In particular, using reactive power from the inverters can both help maintain the voltage levels and improve the grid performance (e.g., reduce power losses) while having a minimal negative impact on the charging station if utilized correctly.

Therefore, a three-layered MPC-based hierarchical control structure was proposed to control an HPCS that consists of different resources and charging demands. Simulations showed how the proposed strategy could improve the grid performance and increase the charging station's profits compared to simpler controllers. It is shown that the daily profits can be further increased by allowing the controller to provide FCR-N services. The controller could also be used to provide other types of ancillary services, e.g., voltage quality improvement or congestion management. However, a Nordic market for FCR-N services already exists, which makes it easier to quantify the potential increase in profits for this ancillary service.

As a part of further work, the proposed controller should be improved to better account for load uncertainties. In this way, the maximum range of flexibility at the HPCS can be predicted with higher accuracy. For such a controller to be even more beneficial for both the DSO and the HPCS, the economic incentives for providing other ancillary services than FCR-N should be investigated in more detail. It will also be important to develop frameworks for better interaction between DSOs and HPCSs. This should include an evaluation of centralized, decentralized and/or autonomous control strategies and the benefit of these strategies as a part of the DSOs' grid operation. This will become even more important when coordinating the flexibility provision from several HPCSs in the same grid area. However, this first requires an intelligent EMS for the HPCSs that can easily adapt to new operating conditions and price signals, which was the aim of this work.

CRediT authorship contribution statement

Jonatan Ralf Axel Klemets: Conceptualization, Methodology, Software, Validation, Investigation, Writing – review & editing, Visualization. **Eirik Haugen:** Methodology, Software, Data curation, Writing – review & editing. **Bendik Nybakk Torsæter:** Resources, Writing – review & editing, Supervision, Project administration, Funding acquisition.

Declaration of competing interest

The authors declare that they have no known competing financial interests or personal relationships that could have appeared to influence the work reported in this paper.

Data availability

Data will be made available on request.

Acknowledgments

The authors gratefully acknowledge the support and contributions from the project consortium of the research project *FuChar - Grid and Charging Infrastructure of the Future*, funded by the industry partners and the Research Council of Norway under Grant (295133/E20). We also want to thank Jon Are Suul and Giuseppe Guidi for valuable input.

References

[1] Lin B, Li Z. Is more use of electricity leading to less carbon emission growth? An analysis with a panel threshold model. Energy Policy 2020;137.
[2] Gambhir A, Rogelj J, Luderer G, Few S, Napp T. Energy system changes in 1.5°C, well below 2°C and 2°C scenarios. Energy Strategy Rev 2019;23:69–80.
[3] Nguyen N, Mitra J. Reliability of power system with high wind penetration under frequency stability constraint. IEEE Trans Power Syst 2018;33(1):985–94.
[4] Fernández-Guillamón A, Gómez-Lázaro E, Muljadi E, Molina-García Á. Power systems with high renewable energy sources: A review of inertia and frequency control strategies over time. Renew Sustain Energy Rev 2019;115.
[5] Du P, Matevosyan J. Forecast system inertia condition and its impact to integrate more renewables. IEEE Trans Smart Grid 2018;9(2):1531–3.
[6] Ivarsøy E. Optimal planning of fast charging stations for EVs – A Norwegian case study. NTNU; 2020.
[7] Fjær KK, Lakshmanan V, Torsæter BN, Korpås M. Heavy-duty electric vehicle charging profile generation method for grid impact analysis. In: 2021 international conference on smart energy systems and technologies. 2021, p. 1–6.
[8] Fanglei LI, Fan W, Jiaming YA, Guoyi XU, Tianshu BI. Estimating maximum penetration level of renewable energy based on frequency stability constrains in power grid. In: Proceedings of 5th Asia conference on power and electrical engineering. 2020, p. 607–11.
[9] Dharmakeerthi CH, Mithulananthan N, Saha TK. Impact of electric vehicle fast charging on power system voltage stability. Int J Electr Power Energy Syst 2014;57:241–9.
[10] Mehammer EB, Berg K, Torsæter BN, Johansson O. Power quality in islanded microgrids supplied by vehicle-to-grid: Norwegian pilot study. In: 2021 IEEE madrid powerTech. 2021, p. 1–6.
[11] Yu R, Chen Y, Huang X, De La Parra HZ. Economic evaluation for EVCS with ancillary service provision capability. In: 2014 IEEE conference and expo transportation electrification Asia-Pacific. 2014, p. 1–5.

[12] Haugen E, Berg K, Torsæter BN, Korpås M. Optimisation model with degradation for a battery energy storage system at an EV fast charging station. In: 2021 IEEE madrid powerTech. 2021, p. 1–6.
[13] Solanke TU, Ramachandaramurthy VK, Yong JY, Pasupuleti J, Kasinathan P, Rajagopalan A. A review of strategic charging–discharging control of grid-connected electric vehicles. J Energy Storage 2020;28.
[14] Khalkhali H, Hosseinian SH. Multi-stage stochastic framework for simultaneous energy management of slow and fast charge electric vehicles in a restructured smart parking lot. Int J Electr Power Energy Syst 2020;116.
[15] Tan H, Chen D, Jing Z. Optimal sizing of energy storage system at fast charging stations under electricity market environment. In: IEEE 2nd int. conference on power and energy applications. 2019, p. 7–10.
[16] Pavic I, Capuder T, Kuzle I. A comprehensive approach for maximizing flexibility benefits of electric vehicles. IEEE Syst J 2018;12(3):2882–93.
[17] Parastvand H, Moghaddam V, Bass O, Masoum MAS, Chapman A, Lachowicz S. A graph automorphic approach for placement and sizing of charging stations in EV network considering traffic. IEEE Trans Smart Grid 2020;11(5):4190–200.
[18] Ma T-Y, Xie S. Optimal fast charging station locations for electric ridesharing with vehicle-charging station assignment. Transp Res D Transp Environ 2021;90:102682.
[19] Sun B. A multi-objective optimization model for fast electric vehicle charging stations with wind, PV power and energy storage. J Clean Prod 2021;288:125564.
[20] Domínguez-Navarro J, Dufo-López R, Yusta-Loyo J, Artal-Sevil J, Bernal-Agustín J. Design of an electric vehicle fast-charging station with integration of renewable energy and storage systems. Int J Electr Power Energy Syst 2019;105:46–58.
[21] Tan KM, Padmanaban S, Yong JY, Ramachandaramurthy VK. A multi-control vehicle-to-grid charger with bi-directional active and reactive power capabilities for power grid support. Energy 2019;171:1150–63.
[22] Ahmed I, Adil HMM, Ahmed S, Ahmad I, Rehman Z. Robust nonlinear control of battery electric vehicle charger in grid to vehicle and vehicle to grid applications. J Energy Storage 2022;52:104813.
[23] Mahfouz MM, Iravani MR. Grid-integration of battery-enabled DC fast charging station for electric vehicles. IEEE Trans Energy Convers 2020;35(1):375–85.
[24] Sun B, Dragičević T, Freijedo FD, Vasquez JC, Guerrero JM. A control algorithm for electric vehicle fast charging stations equipped with flywheel energy storage systems. IEEE Trans Power Electron 2016;31(9):6674–85.
[25] Datta U, Kalam A, Shi J. Smart control of BESS in PV integrated EV charging station for reducing transformer overloading and providing battery-to-grid service. J Energy Storage 2020;28:101224.
[26] Guerrero JM, Vásquez JC, Teodorescu R. Hierarchical control of droop-controlled DC and AC microgrids — a general approach towards standardization. In: 2009 35th annual conference of IEEE industrial electronics. 2009, p. 4305–10.
[27] Wu Y, Wang Z, Huangfu Y, Ravey A, Chrenko D, Gao F. Hierarchical operation of electric vehicle charging station in smart grid integration applications — An overview. Int J Electr Power Energy Syst 2022;139:108005.
[28] Li Y, Li L, Peng C, Zou J. An MPC based optimized control approach for EV-based voltage regulation in distribution grid. Electr Power Syst Res 2019;172:152–60.
[29] Kouka K, Masmoudi A, Abdelkafi A, Krichen L. Dynamic energy management of an electric vehicle charging station using photovoltaic power. Sustain Energy Grids Netw 2020;24:100402.
[30] Kler D, Zabetian Hosseini A, Varghese S, Sun C, Joos G. A rule based EMS for fast charging station with CHIL implementation. In: 2020 IEEE energy conversion congress and exposition. 2020, p. 1319–24.
[31] Mohamed AAS, Jun M, Mahmud R, Mishra P, Patel SN, Tolbert I, et al. Hierarchical control of megawatt-scale charging stations for electric trucks with distributed energy resources. IEEE Trans Transp Electrification 2022.
[32] shafiei M, Ghasemi-Marzbali A. Fast-charging station for electric vehicles, challenges and issues: A comprehensive review. J Energy Storage 2022;49:104136.
[33] Klemets JRA, Torsæter BN. MPC-based voltage control with reactive power from high-power charging stations for EVs. In: 2021 IEEE madrid powerTech. 2021, p. 1–6.
[34] Włodarczyk P, Sumper A, Cruz M. Voltage control of distribution grids with multi-microgrids using reactive power management. Adv Electr Comput Eng 2015;15(1):83–8.
[35] Paudyal S, Ceylan O, Bhattarai BP, Myers KS. Optimal coordinated EV charging with reactive power support in constrained distribution grids. In: Power energy society general meeting. 2017.
[36] Rana R, Torsæter BN. Coordinated voltage support with reactive power from high-power charging stations for EVs. In: 2021 IEEE madrid powerTech. 2021, p. 1–6.
[37] Stock DS, Sala F, Berizzi A, Hofmann L. Optimal control of wind farms for coordinated TSO-DSO reactive power management. Energies 2018;11(1).
[38] Morch AZ, Sæle H, Siface D, Gerard H, Kockar I. Market architecture for TSO-DSO interaction in the context of European regulation. In: 2019 16th international conference on the European energy market. 2019, p. 1–5.
[39] Hu J, Yang G, Ziras C, Kok K. Aggregator operation in the balancing market through network-constrained transactive energy. IEEE Trans Power Syst 2019;34(5):4071–80.
[40] Arrigo F, Bompard E, Merlo M, Milano F. Assessment of primary frequency control through battery energy storage systems. Int J Electr Power Energy Syst 2020;115.
[41] Greenwood DM, Lim KY, Patsios C, Lyons PF, Lim YS, Taylor PC. Frequency response services designed for energy storage. Appl Energy 2017;203:115–27.
[42] Bañol Arias N, Hashemi S, Andersen PB, Træholt C, Romero R. Assessment of economic benefits for EV owners participating in the primary frequency regulation markets. Int J Electr Power Energy Syst 2020;120:105985.
[43] Thingvad A, Ziras C, Marinelli M. Economic value of electric vehicle reserve provision in the nordic countries under driving requirements and charger losses. J Energy Storage 2019;21:826–34.
[44] Khodadadi A, Herre L, Shinde P, Eriksson R, Söder L, Amelin M. Nordic balancing markets: Overview of market rules. In: 17th international conference on the European energy market. 2020, p. 1–6.
[45] Neofytou N, Blazakis K, Katsigiannis Y, Stavrakakis G. Modeling vehicles to grid as a source of distributed frequency regulation in isolated grids with significant RES penetration. Energies 2019;12(4).
[46] Cao Y, Huang L, Li Y, Jermsittiparsert K, Ahmadi-Nezamabad H, Nojavan S. Optimal scheduling of electric vehicles aggregator under market price uncertainty using robust optimization technique. Int J Electr Power Energy Syst 2020;117:105628.
[47] Lee JH. Model predictive control: Review of the three decades of development. Int J Control Autom Syst 2011;9:415–24.
[48] Hu J, Shan Y, Guerrero JM, Ioinovici A, Chan KW, Rodriguez J. Model predictive control of microgrids – An overview. Renew Sustain Energy Rev 2021;136.
[49] Ellis M, Durand H, Christofides PD. A tutorial review of economic model predictive control methods. J Process Control 2014;24(8):1156–78.
[50] Fastned. Fastned charging curve. 2020, Online: https://support.fastned.nl/hc/en-gb. [Accessed 5 August 2020].
[51] Löfberg J. YALMIP: a toolbox for modeling and optimization in MATLAB. In: 2004 IEEE international conference on robotics and automation. 2004, p. 284–9.
[52] Tütüncü RH, Toh KC, Todd MJ. Solving semidefinite-quadratic-linear programs using SDPT3. Math Program Ser B 2003;95(2):189–217.
[53] Musunuru K. Understanding systems of linear equations and programming through lpSolve and R language. 2014.
[54] Mimer. Price statistics for FCR. 2021, Online: https://mimer.svk.se/PrimaryRegulation/PrimaryRegulationIndex. [Accessed 21 April 2021].